EASR

Engineering and Applied Science Research

https://www.tci-thaijo.org/index.php/easr/index

Published by the Faculty of Engineering, Khon Kaen University, Thailand

Recovery of valuable metals from NMC-811 li-ion battery waste with froth flotation and hydrometallurgical extraction

Saddam Husin*[1)], Aghni Ulma Saudi[1)], Galih Taqwatomo[1)], Muhammad Dikdik Gumelar[1)], Jarot Raharjo[2)], Sri Rahayu[1)], Hariaman Prasetyo[1)], Hanif Yuliani[1)], Dita Adi Saputra[1)], Oka Pradipta Arjasa[1)], Agustanhakri[1)], Wahyu Tri Utami[1)], Hikam Angga Saputra[3)], Annisa Ramadhanti Ririanza Putri[4)] and Anne Zulfia Syahrial[3)]

[1)]Research Center for Energy Conversion and Conservation, National Research and Innovation Agency (BRIN), Banten, 15314, Indonesia
[2)]Research Center for Advanced Materials, National Research and Innovation Agency (BRIN), Banten, 15314, Indonesia
[3)]Department of Metallurgy and Materials Engineering, Faculty of Engineering, University of Indonesia, UI New Campus, Depok, 16424, Indonesia
[4)]Departement of Chemistry, Faculty of Sains and Data Analytics, Institut Teknologi Sepuluh Nopember, ITS Campus Sukolilo, Surabaya, 60111, Indonesia

Received 12 May 2023
Revised 19 October 2023
Accepted 7 December 2023

Abstract

In this research, the primary objective is to study the recycling process of spent lithium-ion batteries (LIBs) for the recovery of valuable metals - specifically, nickel, manganese, and cobalt. This is accomplished through a comprehensive hydrometallurgical process that integrates froth flotation, acid leaching, and solvent extraction. The optimization of the flotation phase is a pivotal aspect of this study, with a focus on parameters like particle size and collector concentration. This optimization leads to a remarkable separation efficiency, evident in the recovery of 99.3% of the anode mass in the froth and 78.2% of the cathode mass in the precipitate. Notably, nickel emerges as the standout performer, with an extraordinary extraction efficiency of 99.97%. Nickel precipitates as an ammonium nickel sulfate crystals after solvent extraction due to supersaturation. These findings underscore the considerable potential of froth flotation and hydrometallurgical techniques as a sustainable, low-energy solution for recycling valuable metals sourced from spent LIBs.

Keywords: Acid leaching, Froth flotation, Milling method, Nickel sulfate, Spent li-ion batteries, Solvent extraction

1. Introduction

The rapid adoption of electric vehicles (EVs) in place of conventional fossil fuel-based engines has propelled lithium-ion batteries (LIBs) to the forefront as the primary energy source [1, 2]. However, the widespread proliferation of LIBs is not without concerns, notably their finite lifespan, averaging around 10 years, and the finite resources required for manufacturing new batteries. Recycling spent LIBs emerges as a viable solution with the potential to reduce reliance on virgin raw materials and establish a closed-loop cycle for battery production [2]. The International Energy Agency (IEA) anticipates that material recovery from spent LIBs could satisfy up to 6.5% of the total demand for LIB production by 2030 and a substantial 50% by 2040 [3]. Recycling also holds the promise of reducing EV costs by 20-30% due to savings in battery production expenses [4].

Two predominant techniques for recycling spent LIBs are hydrometallurgical and pyrometallurgical methods. Hydrometallurgy, offering enhanced recovery of all metallic compounds present in spent LIBs, including lithium and aluminum, stands out as a more favorable option compared to pyrometallurgy, which results in material losses in the form of slag [5]. Nonetheless, an intricate pretreatment procedure is essential to optimize recycling efficiency and curtail energy consumption in subsequent steps. Initial physical pretreatment processes, encompassing disintegration, comminution, and separation, are commonplace [6]. Various separation techniques, relying on size, specific gravity, magnetic properties, and electrostatic conductivity, have been explored to achieve the separation of materials from spent batteries. The overarching goal is to obtain high-purity cathode powders from spent LIBs, thus maximizing end-product value while minimizing production costs [7].

Froth flotation, a physicochemical process designed to selectively separate hydrophilic from hydrophobic materials, emerges as a key strategy for isolating cathode and anode powders. This separation mechanism effectively extracts cathode powders from the black mass, leveraging the contrasting surface hydrophobicity of cathode and anode powders. Hydrophobic graphite is entrained within air bubbles and rises to the surface, while hydrophilic cathode powders, composed of ionic crystals with high polarity, remain in the gangue [8, 9]. Graphite, which is naturally hydrophobic, is carried into the air bubbles and floats to the surface. Meanwhile, cathode powder consisting of ionic crystals with high polarity that are hydrophilic will precipitate at the bottom of the froth flotation device [10]. Chemical reagents such as collectors (which increase hydrophobicity for easier separation), frothers (which produce foam), activators (which increase the binding between collectors and desired materials), modifiers (which change the characteristics of the materials),

*Corresponding author.
Email address: sadd001@brin.go.id
doi: 10.14456/easr.2024.13

and depressants (which stop undesirable materials from flotation) can all be added to improve the efficiency of the separation process [11, 12].

The hydrometallurgical extraction techniques for the cathode powders begin with leaching in order to dissolve the metals from the powders once graphite has been thoroughly removed [13]. Depending on the particular components and the intended end-product form, leaching can be done with a range of leaching reagents, including bases, acids, and organic and inorganic solutions [14-16]. Strong acids including nitric acid, hydrochloric acid, and sulfuric acid are frequently used; the selection depends on the desired end result [17]. The ensuing hydrometallurgical processes, such as solvent extraction and solid precipitation, continue to align with the recycling objectives [18].

The core focus of this research centers on the extraction of nickel from spent NMC-811 batteries. The process initiates with the treatment of the black mass derived from battery waste through froth flotation, a method adept at segregating cathode and anode powders. Subsequently, the materials undergo hydrometallurgical extraction, where the efficacy of the froth flotation process is meticulously examined. This comprehensive analysis encompasses the identification of distinct phases present in both the filtrate and the froth. Furthermore, an in-depth scrutiny of the morphology of the cathode and anode powders is conducted to discern any differentiating characteristics. To enhance understanding of the operational dynamics, leaching efficiency is assessed through chemical composition analysis. Notably, the most optimal leaching parameters are subsequently applied as a foundation for advancing to the solvent extraction phase, which inherently targets the separation of nickel from cobalt and manganese constituents. By honing in on the hydrometallurgical approach, optimizing efficiency, and directing attention to the extraction of nickel from NMC-811 batteries, this research distinctly contributes to the field by advancing our understanding of sustainable battery recycling processes. Nevertheless, certain challenges and limitations in current investigations warrant further exploration, potentially uncovering more efficient methods for LIB recycling.

2. Materials and methods

2.1 Initial spent NMC-811

Spent NMC-811 li-ion batteries were discharged using a Rigol DL 3021 discharging machine. Furthermore, it was carried out manually dismantled, and scraped to obtain the electrode powders that are attached to the copper and aluminum collectors. Both the cathode and anode powders were put together as black mass, as the actual condition where the pretreatment procedure is automated yields in the mixed state of electrode powders after crushing and separation process. The black mass was then subjected to ball milling to reduce the particle size with the speed of 1500 rpm for 5 minutes. The milled powders were then sieved to the size of 250 µm and 74 µm then subjected to X-ray fluorescence (XRF) and X-ray diffraction (XRD) tests to evaluate the phase and chemical composition of the black mass.

2.2 Froth flotation

40 grams of electrode powder was added into the flotation bath (Denver Flotation D-12) with 1000 mL of water [19] and stirred for 5 minutes with an impeller speed of 1800 rpm. N-dodecane as a collector with concentration variations of 150 g/t and 450 g/t was added and conditioned for 3 minutes, followed by the addition of methyl isobutyl carbinol (MIBC) as a frother, with concentration of 150 g/t and conditioned for 2 minutes. Flotation process was held for 30 minutes with aeration rate of 2 L/minutes at room temperature (25°C) (Table 1). The flotation products were dried in an oven at 105 °C for 12 hours. Afterwards, the flotation products were analyzed by XRD to confirm the phase and scanning electron microscopy (SEM) to observe the powder morphology. The metal recovery can be calculated with equation (1):

$$\%R = C.\frac{c}{F}.f) \times 100\% \quad (1)$$

Table 1 Design of Experiment for Froth Flotation Process

Electrode powder mass (g)	Particle size (µm)	Collector (g/t)	Frother (g/t)	pH	Floation Process Time (minutes)	Temperature (°C)
40	250	150	150	10	30	25
40	250	300	150	10	30	25
40	250	450	150	10	30	25
40	74	150	150	10	30	25
40	74	300	150	10	30	25
40	74	450	150	10	30	25

Figure 1 illustrates the fundamental concept of froth flotation. This technique plays a pivotal role in segregating valuable minerals from non-valuable minerals or impurities, leveraging variations in hydrophobicity. Hydrophobic particles tend to associate with air bubbles, thus ascending to the surface, while hydrophilic particles settle at the flotation bath's base. The process capitalizes on density disparities between air bubbles and water, facilitating effective mineral separation.

Within the pulp phase, turbulence is induced by an agitator, fostering collisions between particles and bubbles. This dynamic interaction leads to the bonding of hydrophobic particles with bubbles, resulting in the formation of bubble-particle aggregates. These aggregates are subsequently conveyed into the froth phase, facilitating recovery. Significantly, only when mineral particles exhibit a sufficient level of hydrophobicity do, they effectively adhere to air bubbles. Successful attachment of mineral particles to air bubbles exclusively transpires upon their ascent to the pulp's surface, culminating in the establishment of a stable froth. Any premature rupture of air bubbles precludes their capacity to retain mineral particles. To establish this critical state, the deployment of distinct chemical agents, denoted as flotation reagents, becomes imperative [20].

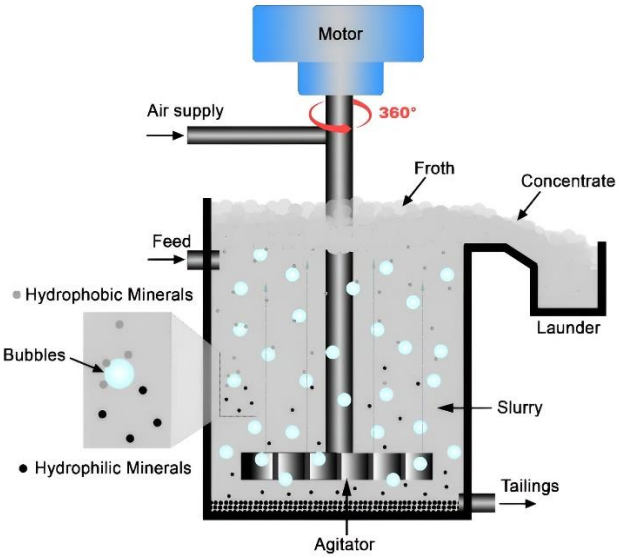

Figure 1 Principles of the flotation process [20]

2.3 Hydrometallurgical extraction

The cathode powder from the previous flotation process was leached using technical H_2SO_4 purchased from PT. Muara Makmur Bersama with concentrations of 1 M and 2 M and technical H_2O_2 as a reduction agent purchased from CV. Karunia Makmur Persada, liquid/solid ratio of 30 mL/g, leaching temperature of 70 °C and leaching time of 90 minutes. The leaching percentage can be calculated with equation (2):

$$X_B = \left(\frac{m1}{m2}\right) \times 100\% \quad (2)$$

Where, X_B was a leaching efficiency, m1 was a metal concentration after leaching, and m2 was a metal concentration before leaching. While the chemical reaction during the leaching process is as followed on equation (3):

$$10LiNi_{\frac{8}{10}}Mn_{\frac{1}{10}}Co_{\frac{1}{10}}O_{2\,(s)} + 15H_2SO_{4\,(aq)} + H_2O_{2\,(aq)} \longrightarrow 8NiSO_{4\,(aq)} + MnSO_{4\,(aq)} + CoSO_{4\,(aq)} + 4Li_2SO_{4\,(aq)} + 16H_2O_{2_{2\,(aq)}} + 3O_{2\,(g)} \quad (3)$$

The first solvent used was Na-Cyanex 272 (bis (2,4,4-trimethyl pentyl) phosphinic acid to separate cobalt manganese in an organic phase solution and nickel lithium in an aqueous phase solution at pH 6. The second solvent used was Na-D2EHPA (di-(2-ethyl hexyl) phosphoric acid) to separate cobalt in the organic phase and manganese in the aqueous phase at pH 2.95. Ammonia is added to adjust the pH as required in the solvent extraction stage. The two solvents were obtained from the results of the saponification reaction. The reaction of the saponification process can be written as follows (4-5)

$$Na^+_{(aq)} + \frac{1}{2}(HA)_{2\,(org)} \longrightarrow NaA_{(org)} + H^+_{(aq)} \quad (4)$$

$$M^{2+}_{(aq)} + NaA_{(org)} + 2(HA)_{2(org)} \leftrightarrow (MA_2 \cdot 3HA)_{(og)} + Na^+_{(aq)} + H^+_{(aq)} \quad (5)$$

The medium used in the extractant is kerosene. The separation process between the organic and aqueous phases lasted 30 minutes in a separatory funnel. The percentage of metal extraction (%E) can be calculated through the distribution ratio (D) between the organic and aqueous concentrations can be written as follows (6).

$$D = \frac{(C_0 - C)}{C} \times \frac{V_{air}}{V_{org}} \quad (6)$$

$$\%E = \frac{D}{\left(D + \frac{V_{air}}{V_{org}}\right)} \times 100\% \quad (7)$$

Where, C_0 is the initial concentration of metal ions in the aqueous phase, C is the equilibrium concentration of metal ions in the aqueous phase, and V_{air}/V_{org} is the volume ratio of the aqueous phase and organic phase.

After the extraction step, the organic phase solution was stripped using H_2SO_4 with a concentration of 0.2 M for 30 minutes, and the separation time that occurred was 30 minutes. The first stripping process aims to separate cobalt manganese and Na-Cyanex272 + Cyanex, where the solvent can be reused in an organic phase. The second stripping process is to separate manganese and Na-D2EHPA + D2EHPA, where the solvent can also be reused in the organic phase. Stripping efficiency can be calculated through equation (7). Each solution from the leaching process, solvent extraction stage 1 and solvent extraction stage 2 was partially taken for AAS analysis. Figure 2 demonstrates all of stages of extraction process included mechanical, froth flotation and hydrometallurgical process in this study.

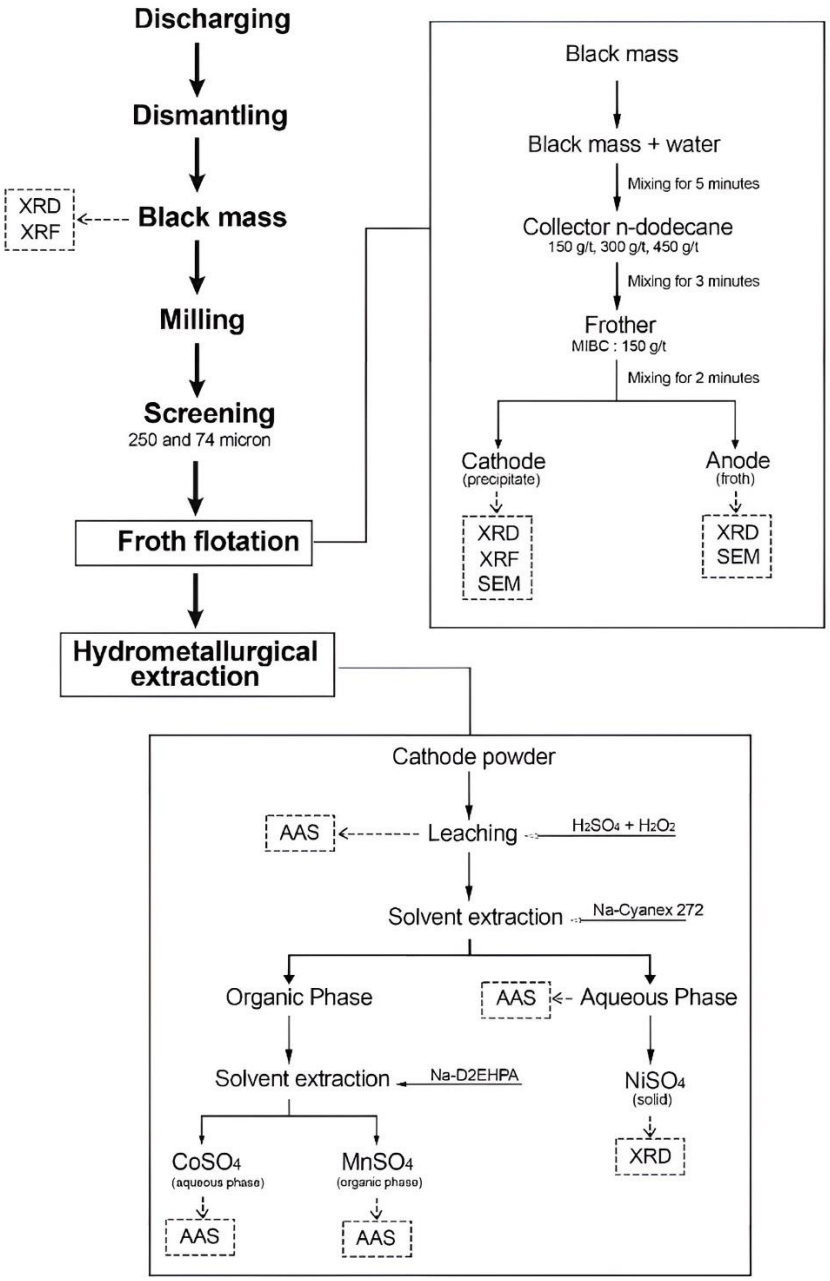

Figure 2 Stages of extraction spent NMC-811 li-ion batteries process

3. Result and discussion

3.1 Initial spent battery

Black mass consisting of cathode and anode obtained from spent NMC-811 li-ion batteries. Before the flotation process, the black mass was grinding and sieving. The grinding process, which utilizes horizontal shear forces and vertical rolling pressure, aims to unbind the electrode material from the foil, which cannot be carried out in the screening process. That process resulted in 2 different sizes of particles (250 μm and 74 μm) so that it can determine the difference in buoyancy between the two particle sizes.

XRF analysis was applied to the black mass intended for flotation feed to scrutinize the elemental composition across distinct particle sizes. Figure 3 depicts the elemental content of Ni, Mn, Co, Li, and Al derived from the cathode. Between the two particle sizes catagory, the 250 μm category exhibited heightened concentrations of valuable constituents (Ni, Mn, and Co). Notably, within the 250 μm particle size, Ni emerged as the predominant element, constituting 39.7% of the mass, in stark contrast to the remaining particles, which accounted for merely 13.8%. Additionally, marginal amounts of Mn, Co, and Al were also detected. Aluminum impurities persisted across both particle sizes, hinting at residual attachment despite the grinding process. This phenomenon can be attributed to the persistent presence of polyvinylidene fluoride (PVDF) as an organic binder, which complicates the complete detachment of flotation feed from the electrode material [21]. Notably, as per existing research [22], XRF analysis encounters limitations when applied to light metal groups characterized by shallow light exposure and long-wavelength attributes, rendering elements like Li and C undetectable via XRF methodologies.

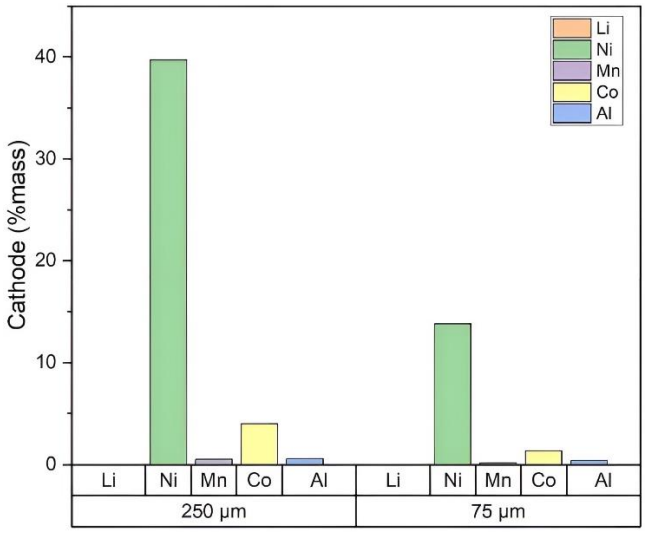

Figure 3 The distribution of elemental content in different particle sizes

The black mass was tested using XRD to analyze the phase of the material and identify contents of lithium (Li) and carbon (C), which cannot be detected from XRF. Based on an XRD graph (Figure 4) that shows two components consisting of $Li_{2,88}Mn_{2,22}O_6$ and graphite (C4) that represents cathode and anode, respectively. The graphene (C4) hit the highest peak at 26.56θ, and the second peak appeared at 58.62θ, while the rest of the peaks is $Li_{2,88}Mn_{2,22}O_6$, with the most extended peak at 18.7θ. The percentage of $Li_{2,88}Mn_{2,22}O_6$ and graphite (C_4) based on the XRD pattern are 24.7 and 75.3, respectively. Different peaks that clarify no significant effect from different particle sizes have yet to be seen.

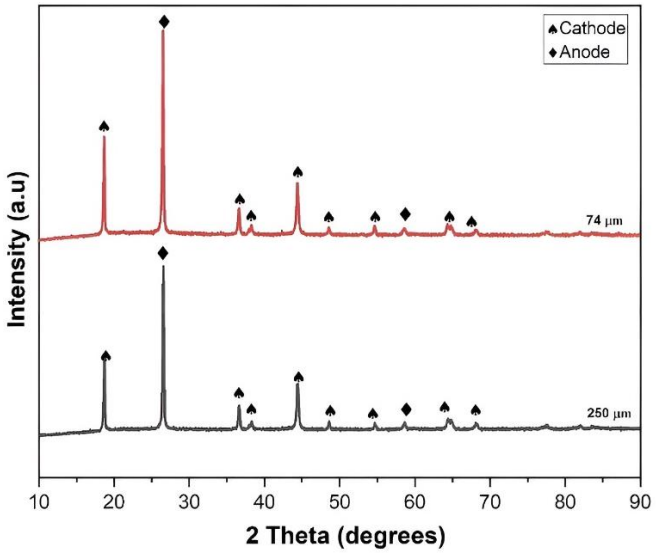

Figure 4 XRD pattern of spent NMC-811 black mass

3.2 Froth flotation

The batch system was used in the flotation process to maximize the separation between the cathode and anode. The chemical reagents used to create conditions for the flotation process to occur correctly are the collector and frother. In addition, other chemical reagents, namely modifiers, play an essential role in the flotation process by functioning to adjust the environment to suit the flotation environment. Based on surface properties, the anode is hydrophobic, binding to air bubbles and being lifted to the surface to form foam products. At the same time, the cathode material will tend to remain at the bottom of the flotation tub because it has hydrophilic properties. There are impurity materials such as PVDF as an organic binder that binds electrode particles to the foils makes it difficult to remove them with just mechanical force, which leaves some of the electrode material on the foils and reduces recovery [21]. The PVDF forms a layer that causes air bubbles, and excellent adhesion of flotation products (graphite) does not occur. The anode surface, covered with PVDF layers, causes no contact between the anode and air bubbles so that they cannot arise to the surface and tend to be in solution (middling) and precipitate together with the cathode thus that the efficiency of obtaining anode is tiny.

Figure 5 (a-b) illustrates the flotation product phases resulting from three distinct collector masses across two varying particle sizes. In the case of the samples with 250 µm particle size, the froth phase remained absent for collector concentrations of 150 g/t and 300 g/t, only manifesting at a concentration of 450 g/t—a contrast to the behavior observed in the 74 µm particle size. The presence of a 0% percentage highlights suboptimal separation under these collector concentrations when dealing with a 250 µm particle size. This phenomenon can be attributed to the influence of the organic binder (PVDF), which impairs separation efficiency by generating a protective layer on the anode surface, inhibiting effective adhesion between the anode and air bubbles.

Furthermore, the selection of the frother type also exerts an impact, particularly concerning larger particle sizes. The frother variant, Methyl isobutyl carbinol (MIBC), exhibits relatively modest frothing efficacy and limited air bubble persistence. Consequently, it is less suited for larger particle sizes due to its inability to maintain bubble stability upon collision with particles, rendering it susceptible to rupture.

Excessive particle sizes lead to heightened associations between particles and air bubbles, surpassing the density of water. This results in inadequate buoyancy, causing particles to still precipitate. Moreover, the interplay between air bubbles and particles engenders three consecutive subprocesses—collision, attachment, and release [23]. To facilitate effective adhesion, each particle must navigate within the capture radius, enabling collision upon the ascending air bubble's surface. Subsequently, particles adhere and migrate along the bubble's surface until an angle of approximately 60˚ to 90˚ with respect to the vertical axis of the bubble's geometry is attained. At this juncture, bubble-particle aggregates form and ascend toward the surface, coalescing into a froth. The attachment of particles to bubbles hinges on adhesion forces at the three-phase contact lines—solid-liquid, solid-gas, and liquid-gas interfaces—significantly influencing the process.

For larger particle sizes, an augmented collector concentration is requisite to facilitate the adhesion of air bubbles and the transportation of graphite particles to the froth. This augmentation amplifies particle hydrophobicity. Notably, the collector also exhibits a propensity to form bonds with cathode particles. As a result, cathode materials are entrained toward the froth, albeit in minimal quantities. This trend is observed in both particle sizes, with a slight reduction in cathode content within the precipitate phase. At equivalent recovery levels, finer particles yield purer products compared to coarser counterparts. A minor proportion of anode particles cannot achieve flotation due to surface oxidation. However, employing fine grinding techniques eradicates oxidized surface groups, exposing a renewed hydrophobic surface conducive to facile graphite flotation [9].

The preeminent flotation product materializes in the form of a 74 μm particle size in conjunction with a 150 g/t collector concentration. This configuration yields remarkable outcomes, with the froth phase comprising 99.3% anode mass and the precipitate phase containing 78.2% cathode mass. Notably, these anode and cathode compositions outshine similar studies, registering at 90.25% and 35.99%, respectively [9].

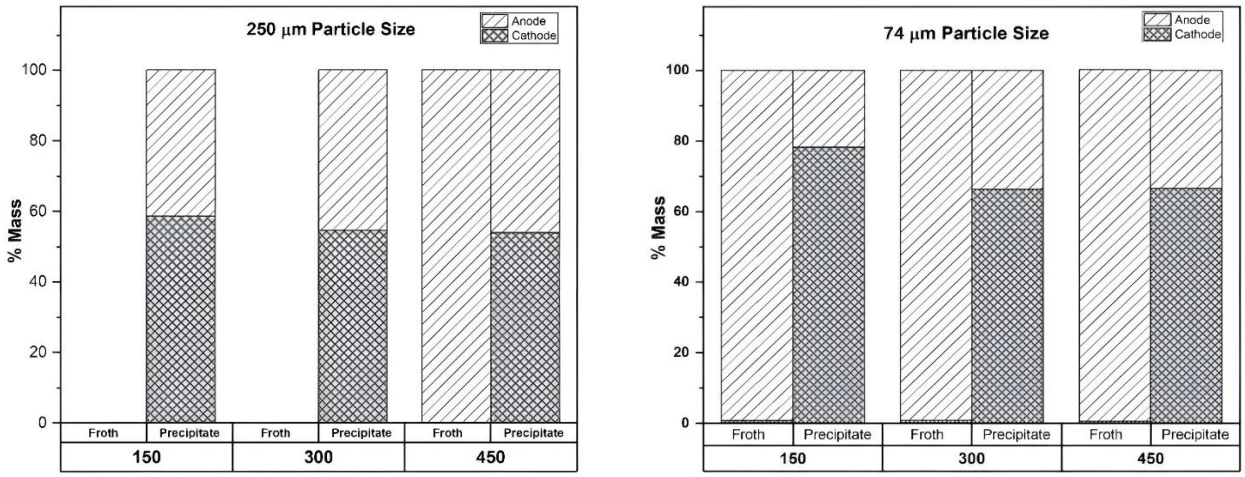

Figure 5 The composition of the flotation product compounds; a. 250 μm; b. 74 μm

The XRD pattern of the hydrophobic material from the froth flotation process dominated by graphite material can be shown in Figure 6. The sharp and tight peak at 26.4 and another small peak at 54.4 degrees correspond to the planes (002) and (004), respectively. The data shows the typical crystal structure of graphite carbon (JCPDS#00-008-0415). The intercellular spacing in the crystal (d_{hkl}) in plane 002 is 3.4 Å. Longitudinal dimension (L_a) of the structural elements is reflected (100) and (101), for which $2\theta \approx 42.32$ and 44.38 [24, 25]. Similar peaks from two collector masses indicate the exact structure of graphite carbon.

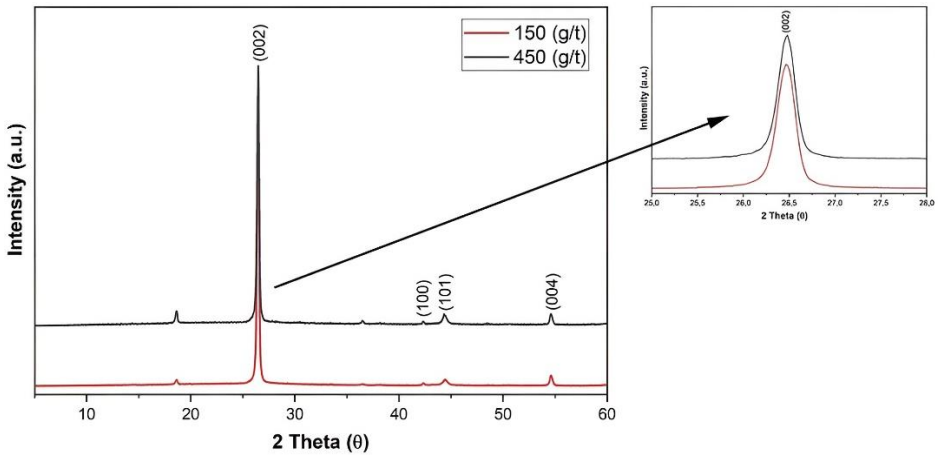

Figure 6 XRD pattern of graphite carbon in hydrophobic material from the flotation process at different collector masses.

Figure 7 shows the surface morphology to particle distribution in the froth and precipitate product using the back scattering method. The cathode compounds containing Ni, Mn, and Co with high atomic numbers will show a bright particle pattern, while the anode compound (graphite), a light element, will appear with a dark particle pattern. Figure **7** (A1), with magnification 500×, is a froth product with 99.3% of graphite, and Figure 7 (B1) is the precipitate product with 78.2% of the cathode, with some still having graphite particles. Almost all anode (graphite) could be separate from the cathode. However, some of the anode particles are also still in the precipitate. These phenomena happen because of two things. The first is the influence of the binder-interfering material (PVDF), which causes the anode to be challenging to float so that it is in the precipitate. The other reason is the grinding process with a ball mill which causes some of the anode and cathode to stick together in a particle.

The grinding procedure engenders both horizontal shear forces and vertical pressure upon particle surfaces. This combined effect triggers the adhesion of certain cathode and graphite anode particles, as visually depicted in Figure 7 (A2) at a magnification of 8000. Remarkably, enhanced hydrophobicity of cathode particles induces their attachment to graphite, subsequently leading to their flotation to the foam-air bubble interface during the flotation process. Figure 7 (B2) underscores that certain cathode particles become enveloped by anode material; an outcome attributed to grinding's impact. This phenomenon hampers the flotation capability of the anode (graphite). Furthermore, the exertion of horizontal shear forces and vertical pressure prompts the internal structure of graphite to slide and flake along its layered configuration. This dynamic generates novel hydrophobic surfaces, augmenting flotation propensity [26].

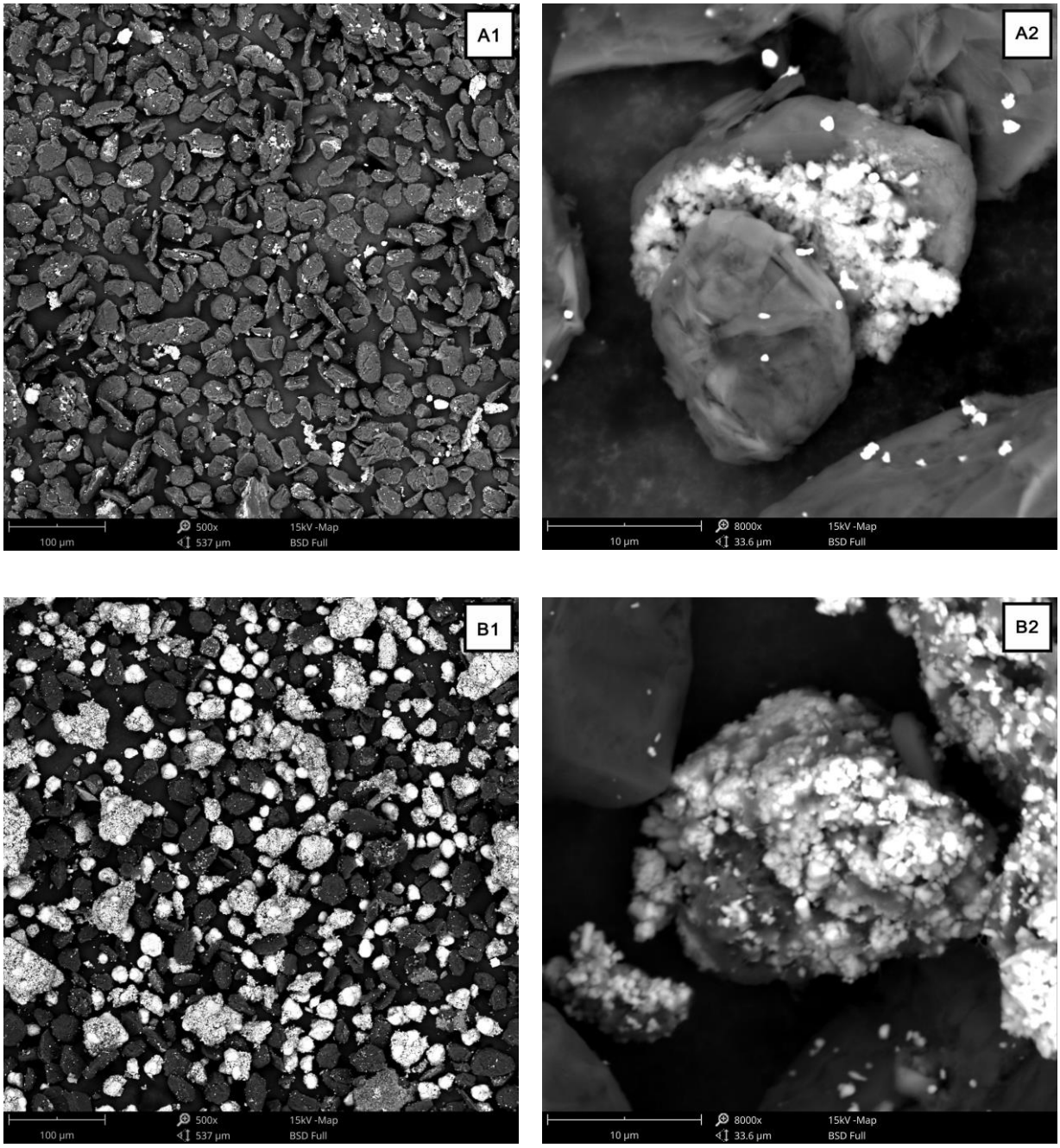

Figure 7 SEM images of forth flotation product with collector 450 g/t and particle size 74 µm (A1) Froth phase magnification 500×, (A2) Froth phase magnification 8000×, (B1) Precipitate phase magnification 500×, (B2) Precipitate phase magnification 8000×)

3.3 Hydrometallurgical extraction

Hydrophilic materials dominated by cathode materials are used in hydrometallurgical processes. It was first analyzed by XRF which resulted in a metal composition contained in the cathode concentrate in the form of nickel, manganese and cobalt at 30.6, 0.38 and 3.12 %wt, respectively (Figure 8). The large nickel content is due to the source of the used battery which is NMC 811 battery with a large nickel content.

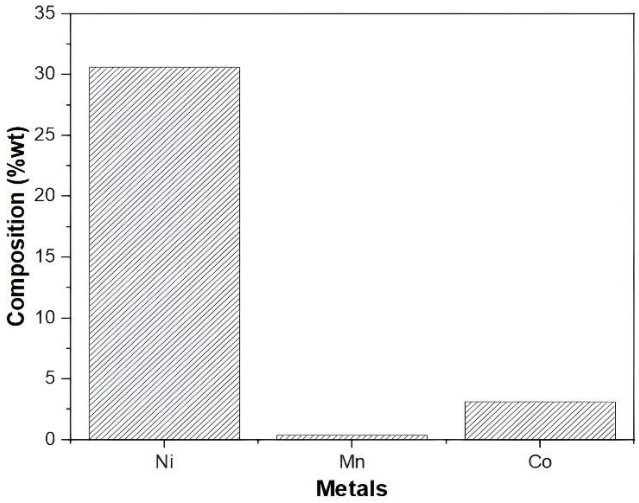

Figure 8 Ni, Co, and Mn composition analysis in the leach feed of the cathode

Selective leaching of heavy metals in cathode powder demonstrated improvement of metal contents, with leaching efficiency data presented on Figure 9. Result shows leaching with 2 M of H_2SO_4 as the reagent has the highest leaching efficiency from all the metals compared to that of lower molarity. The percentage recovery at 2 M H_2SO_4 of nickel, manganese and cobalt metals were 47.65, 25.80, and 24.37%, respectively. The molar concentration of acid led to an increase in leaching efficiency. Similar behavior was shown by Mn, Ni, and Co, and their leaching efficiency increased with acid concentration and leaching duration [1]. The increase of acid concentration can induce the intensification of leaching efficiency, yet, if the acid concentration is too high, it will confine the diffusion of leached products [27]. Temperature of 70 ºC is the ideal condition for leaching procedure, as higher reaction temperature can escalate the leaching kinetics. However, if the temperature is too high, it can lead to the decomposition of acids and reductants, which will cause the reduction of leaching efficiency [27]. Leaching time of 90 minutes is also considered efficient for a reaction between particles and leaching reagent to happen [15]. Besides, stirring the solution during the leaching process can accelerate the dissolution of cathode powder and increase the effectiveness.

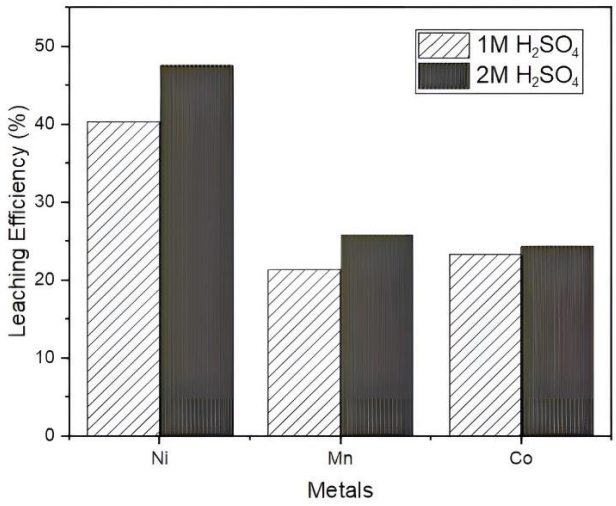

Figure 9 Leaching efficiency of Ni, Co, and Mn with varying acid concentrations

Solvent extraction is an essential step after the leaching process, mainly to separate nickel and cobalt, as nickel and cobalt have similar physio-chemical properties in aqueous solution, making it necessary for them to be separated before undergoing further treatment [15]. Solvent extraction is preferred compared to other techniques owing to its advantages, as it is cost-efficient and results in high purity products [28]. The most common reagents used for solvent extraction include D2EHPA, PC88A, Cyanex272, Versatic10, and LIX 84-IC [29].

D2EHPA can effectively isolate cobalt from manganese, while Cyanex 272 demonstrates a pronounced preference for separating nickel from cobalt. However, the effectiveness of this separation is limited when dealing with a target material containing all four metals, namely nickel, cobalt, manganese, and lithium. Initially, the separation of nickel and cobalt is carried out using Na-Cyanex

272, as a substantial quantity of both cobalt and nickel is present in the NMC cathode waste material. Failure to perform this preliminary nickel-cobalt separation can lead to challenges in achieving high product purity and may hinder the subsequent processing steps [15].

The initial extraction phase employing Na-Cyanex 272 effectuates the segregation of nickel and lithium from manganese and cobalt. Consequently, nickel and lithium remain within the aqueous phase, while manganese and cobalt find refuge in the organic phase. Subsequently, the organic phase derived from the initial extraction stage proceeds to the subsequent extraction stage. In the subsequent step of extraction, Na-D2EHPA is employed to effectuate the separation of manganese and cobalt. This procedure leads to manganese entering the organic phase, whereas cobalt persists within the aqueous phase. The aqueous phase containing nickel from the initial extraction step, the organic phase holding manganese, and the aqueous phase housing cobalt from the second extraction step undergo AAS analysis to ascertain their composition.

The resultant recovery rates of nickel, manganese, and cobalt are graphically depicted in Figure 10. Impressively, nickel attains the pinnacle of recovery at 99.97%, while manganese and cobalt achieve recoveries of 64.69% and 59.35%, respectively. Notably, the recovery percentage of nickel from the first-stage extraction surpasses analogous studies, standing at 97.88% [28].

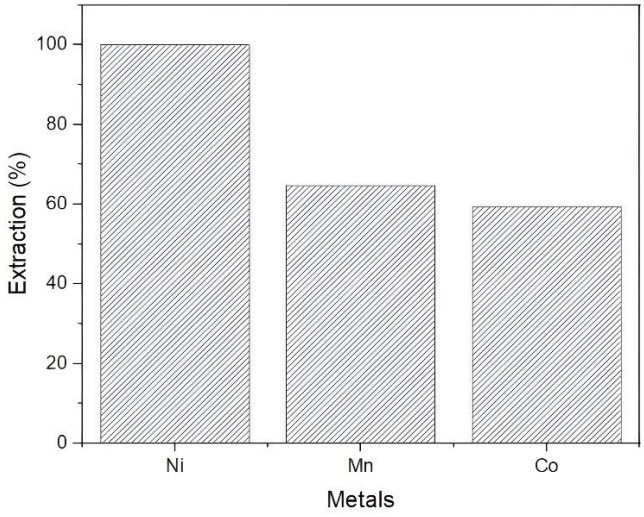

Figure 10 Ni, Co, and Mn recovery percentages in different solutions

Nickel in the aqueous phase crystallized into nickel complex crystals with a light green color (Figure 11). This phenomenon happened due to the high nickel content in the solution, as feed of NMC-811 battery was used, which led to supersaturation. Sist and Demopoulos [30] in their work mentioned that this situation is possible to occur when supersaturated nickel hydroxide solution is treated on certain conditions, with variation of pH and temperature. They also stated the pH of 6.73 can generate homogeneous precipitation of nickel hydroxide in aqueous sulfate media. This experiment uses pH of 6 in the first solvent extraction with Na-Cyanex272, which can promote precipitation of the aqueous solution.

Figure 11 Nickel complex crystals after solvent extraction process

The XRD results of the nickel complex crystals are presented in Figure 12. It can be seen that there is an ammonium nickel sulfate component (ICCD#01-078-1838) where the chemical formula is $(NH_4)_2$ (Ni $(H_2O)_6$) $(SO_4)_2$ and the crystal system is monoclinic. Crystal planes of ammonium nickel sulfate are (011), (120) (12$\underline{1}$), (20$\underline{1}$), (130) (220) (13$\underline{1}$), and (11$\underline{2}$) in 2 Theta (degrees) position at 19.14, 20.26, 24.4, 24.86, 27.61, 28,86, 30,75, 34,35, respectively. Based on the XRD results, it is known that the nickel complex crystals obtained is an ammonium nickel sulfate compound. Sulfate and ammonium components in $NiSO_4$ from the leaching step and pH adjusting in solvent extraction could be removed with the other process.

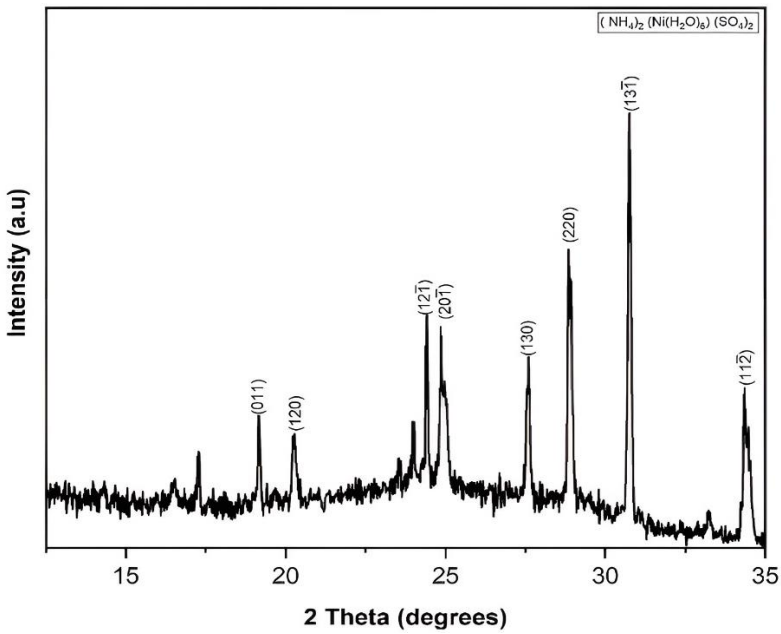

Figure 12 XRD pattern of nickel complex crystals after solvent extraction process

4. Conclusions

In this investigation, the extraction and separation of valuable metals were effectively realized through the integration of froth flotation and hydrometallurgical methodologies. The initial phase harnessed froth flotation as a robust avenue for segregating cathode and anode constituents. Anodal material derived from this process exhibited a commendable structural integrity, as corroborated by XRD analysis. Remarkably, the 74 μm particle size emerged as the optimal condition, yielding the highest separation efficacy, with collector mass variations evincing negligible impact. To enhance separation outcomes, pre-floatation removal of the polymer binder is recommended.

The subsequent hydrometallurgical step, underpinning the separation of valuable cathode elements, prominently excelled in extracting nickel, manifesting a remarkable 99.97% extraction rate. NMC 811, characterized by a significant nickel proportion, readily precipitates into solid NiSO4 from aqueous solutions. Prospective research avenues should concentrate on refining cobalt and manganese extraction percentages, seeking efficacious strategies. In summation, the amalgamation of froth flotation and hydrometallurgy not only expedites the recovery of valuable metals but also does so in an energy-efficient manner, facilitated by uncomplicated equipment.

5. Acknowledgements

The authors would like to acknowledge the Agency for Assessment and Application of Technology (BPPT) Indonesia for the financial support of the DIPA Project Inovation of Energy Storage and Battery Recycling Technology to conduct this research.

6. References

[1] Vieceli N, Casasola R, Lombardo G, Ebin B, Petranikova M. Hydrometallurgical recycling of EV lithium-ion batteries: effects of incineration on the leaching efficiency of metals using sulfuric acid. Waste Manag. 2021;125:192-203.
[2] Benjamasutin P, Promphan R. Recycling of lithium-ion batteries. Determination of optimal parameters for the application of hydrogen peroxide as reducing agent in the leaching process [thesis]. Gothenburg: Chalmers University of Technology; 2020.
[3] International Energy Agency (IEA). The role of critical world energy outlook special report minerals in clean energy transitions. USA: International Energy Agency; 2022.
[4] Melin HE. State of the art in reuse and recycling of lithium-ion batteries-a research review. London: Circular Energy Storage; 2019.
[5] Assunção J. Hydrometallurgical processing of Li-ion batteries from electric vehicles [thesis]. Lisbon: University of Lisbon; 2019.
[6] Samarukha I. Recycling strategies for end-of-life li-ion batteries from heavy electric vehicles [thesis]. Sweden: KTH Industrial Engineering and Management; 2020.
[7] Ye Z, Qiu L, Yang W, Wu Z, Liu Y, Wang G, et al. Nickel-rich layered cathode materials for lithium-ion batteries. Chem Eur J. 2021;27(13):4249-69.
[8] Folayan TO, Lipson AL, Durham JL, Pinegar H, Liu D, Pan L. Direct recycling of blended cathode materials by froth flotation process. Energy Technol. 2021;9(10):1-26.
[9] Zhan R, Oldenburg Z, Pan L. Recovery of active cathode materials from lithium-ion batteries using froth flotation. Sustain Mater Technolo. 2018;17:1-9.
[10] Hu Q, Xu L. An overview on lithium-ion batteries recycling processes. J Phys Conf Ser. 2021;1885:032031.
[11] Verdugo L, Zhang L, Saito K, Bruckard W, Menacho J, Hoadley A. Flotation behavior of the most common electrode materials in Lithium-ion batteries. Sep Purif Technol. 2022;301:121885.
[12] Vanderbruggen A. Lithium-ion batteries recycling with froth flotation – a study on characterization and liberation strategies [thesis]. Helsinki: Aalto University; 2022.

[13] Wang S, Tian Y, Zhang X, Yang B, Wang F, Xu B, et al. A review of processes and technologies for the recycling of spent lithium-ion batteries. IOP Conf Ser Mater Sci Eng. 2020;782:022025.
[14] Xuan W, Otsuki A, Chagnes A. Investigation of the leaching mechanism of NMC 811 ($LiNi_{0.8}Mn_{0.1}Co_{0.1}O_2$) by hydrochloric acid for recycling lithium ion battery cathodes. RSC Adv. 2019;9(66):38612-8.
[15] Chen WS, Ho HH. Recovery of valuable metals from lithium-ion batteries NMC cathode waste materials by hydrometallurgical methods. Metals. 2018;8(5):1-16.
[16] Bai Y, Muralidharan N, Sun YK, Passerini S, Whittingham MS, Belharouak I. Energy and environmental aspects in recycling lithium-ion batteries: concept of battery identity global passport. Mater Today. 2020;41:304-15.
[17] Neumann J, Petranikova M, Meeus M, Gamarra JD, Younesi R, Winter M, et al. Recycling of lithium-ion batteries—current state of the art, circular economy, and next generation recycling. Adv Energy Mater. 2022;12(17):1-26.
[18] Alipanah M, Saha AK, Vahidi E, Jin H. Value recovery from spent lithium-ion batteries: a review on technologies, environmental impacts, economics, and supply chain. Clean Technol Recycl. 2021;1(2):152-84.
[19] Ji Y, Kpodzro EE, Jafvert CT, Zhao F. Direct recycling technologies of cathode in spent lithium-ion batteries. Clean Technol Recycl. 2021;1:124-51.
[20] Wills BA, Finch JA. Chapter 12 - Froth flotation. In: Wills BA, Finch JA, editors. Wills' Mineral Processing Technology. 8th ed. Amsterdam: Elsevier; 2016. p. 265-380.
[21] Zhang G, Du Z, He Y, Wang H, Xie W, Zhang T. A sustainable process for the recovery of anode and cathode materials derived from spent lithium-ion batteries. Sustainability 2019;11(8):2363.
[22] Zawisza B, Sitko R. Determination of lithium in mineral water samples by x-ray fluorescence spectrometry. Appl Spectrosc. 2011;65(10):1218-21.
[23] Nguyen AV, Evans GM. Attachment interaction between air bubbles and particles in froth flotation. Exp Therm Fluid Sci. 2004;28(5):381-5.
[24] Popova AN. Crystallographic analysis of graphite by x-ray diffraction. Coke Chem. 2017;60(9):361-5.
[25] Li ZQ, Lu CJ, Xia ZP, Zhou Y, Luo Z. X-ray diffraction patterns of graphite and turbostratic carbon. Carbon. 2007;45(8):1686-95.
[26] Yu J, He Y, Ge Z, Li H, Xie W, Wang S. A promising physical method for recovery of $LiCoO_2$ and graphite from spent lithium-ion batteries: grinding flotation. Sep Purif Technol. 2018;190:45-52.
[27] Or T, Gourley SWD, Kaliyappan K, Yu A, Chen Z. Recycling of mixed cathode lithium-ion batteries for electric vehicles: current status and future outlook. Carbon Energy. 2020;2(1):6-43.
[28] Tang YC, Wang JZ, Shen YH. Separation of valuable metals in the recycling of lithium batteries via solvent extraction. Minerals. 2023;13(2):1-12.
[29] Alvial-Hein G, Mahandra H, Ghahreman A. Separation and recovery of cobalt and nickel from end of life products via solvent extraction technique: A review. J Clean Prod. 2021;297:1-26.
[30] Sist C, Demopoulos GP. Nickel hydroxide precipitation from aqueous sulfate media. JOM. 2003;55:42-6.